Energy Reports 13 (2025) 3929–3945

Contents lists available at ScienceDirect

Energy Reports

journal homepage: www.elsevier.com/locate/egyr

Research paper

Optimization of ground material properties for enhanced solar chimney power plant efficiency: A CFD and RSM approach

Essam M. Abo-Zahhad [a,b], Ahmed Amine Hachicha [c,d], Mahmoud Z. Mistarihi [a,e], Mohamed H. Salim [b,f,*], Mohamed F.C. Esmail [b]

[a] Department of Mechanical and Industrial Engineering, Liwa College, Abu Dhabi, 41009, United Arab Emirates
[b] Mechanical Power Engineering Department, Faculty of Energy Engineering, Aswan University, Aswan 81528, Egypt
[c] Sustainable and Renewable Energy Engineering Department, University of Sharjah, PO Box 27272, United Arab Emirates
[d] Sustainable Energy and Power System Research Centre, Research Institute for Science and Engineering, University of Sharjah, UAE
[e] Industrial Engineering Department, Faculty of Hijjawi for Engineering Technology, Yarmouk University, Irbid, 21163, Jordan
[f] Institute of Ecology, Technische Universität Berlin, Berlin, 10587, Germany

ARTICLE INFO

Keywords:
Solar Chimney Power Plant
Response Surface Methodology
Optimization
Sustainable Energy

ABSTRACT

Ground thermal properties impact the efficiency and reliability of Solar Chimney Power Plants, yet the dynamic impact of these properties needs more consideration. This study addresses the optimization of SCPP efficiency by investigating the effect of ground materials properties on collector efficiency, updraft velocity, and temperature rise. To this end, we used a combined CFD and Response Surface Methodology (RSM) approach. Numerical simulations, validated against the Manzanares prototype, were performed, followed by regression modeling and material optimization using RSM. Weather data from Aswan, Egypt, spanning July 2021 to June 2024, were used to evaluate annual performance under realistic conditions. Results show that higher ground thermal conductivity and specific heat enhance system efficiency, achieving a collector efficiency of up to 39.11 % and an updraft velocity of 14.63 m/s during peak solar radiation. Optimized configurations improved updraft velocity by 4.62 % under low solar radiation and 4.22 % under high conditions, while power output increased by 17.71 % and 11.05 %, respectively. These findings highlight the important role of optimized ground properties in enhancing performance, particularly under low solar radiation conditions.

1. Introduction

Solar chimney power plants (SCPPs), also known as solar updraft towers, are emerging as a promising solution for sustainable and large-scale electricity generation, particularly in regions with abundant solar resources. These systems utilize solar radiation to drive buoyancy-induced airflow, which is converted into electricity. In recent years, they also offer a renewable alternative to fossil fuels. Particularly, the global energy landscape has been shaped by escalating geopolitical tensions, which have disrupted energy markets and highlighted the vulnerabilities of fossil fuel dependence. The energy crises triggered by these geopolitical conflicts have highlighted the urgent need for clean, resilient, and locally sourced energy technologies that can ensure energy security while addressing environmental challenges. With approximately 1.1 billion people worldwide still lacking access to reliable electricity (Mebarki et al., 2022a), SCPPs hold significant potential to contribute to a sustainable energy future by utilizing solar energy in a cost-effective and scalable manner (Biswas et al., 2023).

The SCPP system consists of three main components: a transparent collector, a ground surface that absorbs solar energy, and a central chimney. Solar radiation heats the air under the collector, creating a temperature difference that drives buoyancy-induced airflow through the chimney. Turbines installed at the chimney base convert the kinetic energy of the airflow into electricity (Pradhan et al., 2021; Krumar Mandal et al., 2022). Early studies on SCPPs were pioneered by Haaf et al. (Haaf, 1984; Haaf et al., 1983), who developed a prototype plant in Manzanares, Spain. The insights gained from this prototype have provided a foundational basis for validating subsequent experimental and computational studies (Cuce et al., 2020).

Research on SCPPs has explored various design and operational factors affecting their performance. For instance, the impact of turbine characteristics, collector and chimney dimensions, and heat flux on

* Corresponding author at: Institute of Ecology, Technische Universität Berlin, Berlin 10587, Germany.
E-mail address: salim@tu-berlin.de (M.H. Salim).

https://doi.org/10.1016/j.egyr.2025.03.035
Received 19 December 2024; Received in revised form 6 March 2025; Accepted 24 March 2025
Available online 28 March 2025
2352-4847/© 2025 The Author(s). Published by Elsevier Ltd. This is an open access article under the CC BY license (http://creativecommons.org/licenses/by/4.0/).

power generation has been widely studied (Esmail and Mekhail, 2019; Yapıcı et al., 2020; Esmail et al., 2021; Toghraie et al., 2018; Hassan et al., 2018). Other investigations have examined external meteorological parameters such as ambient crosswinds and variations in solar radiation (Esmail et al., 2022). Furthermore, thermal energy storage (TES) systems have emerged as a crucial component in SCPPs, enabling the storage of solar energy absorbed by the ground during the day and its release during nighttime or cloudy periods. Effective TES systems can significantly enhance the system's ability to generate electricity consistently throughout the day and across seasons, thereby improving reliability and efficiency (Ikhlef et al., 2022a).

While substantial progress has been made in understanding the factors influencing SCPP performance, several limitations remain. Research on TES systems has often relied on simplified theoretical or experimental models that treat the ground beneath the collector as a uniform bulk material. This approach overlooks the detailed interactions between ground material properties—such as thermal conductivity, specific heat capacity, and density—and critical SCPP performance metrics, including collector efficiency, updraft velocity, and air temperature rise.

For instance, Al-Azawiey and Hassan (Al-Azawiey and Hassan, 2016) compared various materials, including ceramics and black stones, as potential TES candidates, in order to highlight their ability to improve power production. Similarly, Hurtado et al. (Hurtado et al., 2012) demonstrated the impact of soil compaction and thermal inertia on energy output. They revealed a 10 % increase in power generation with higher compaction levels. Computational studies, such as those by Yaswanthkumar and Chandramohan (Yaswanthkumar and Chandramohan, 2019) have explored the use of TES materials through 3D Computational Fluid Dynamics (CFD) models, but their analyses often lack comprehensive optimization frameworks. Experimental studies, like those by Ikhlef et al. (Ikhlef et al., 2022a) have further emphasized the significance of TES in enhancing collector efficiency and overall performance.

Recent studies have continued to advance the understanding of SCPP performance and TES integration. For instance, Mamgain et al. (Mamgain et al., 2024) conducted a CFD investigation into thermal energy storage in a solar chimney power plant by treating the thermal storage layer as a porous material. Their results revealed that materials with higher thermal conductivity, such as sand, are better suited for the thermal storage unit due to their enhanced ability to absorb heat during daylight hours. Ikhlef et al. (Ikhlef et al., 2022b) experimentally studied the effect of various TES systems on the performance of a small-scale SCPP in Isparta, Turkey, with a chimney height of 4.2 m and a collector diameter of 5.93 m. Their findings demonstrated that collector efficiency strongly depends on thermal storage, with crushed gravel emerging as the best TES material. They reported a collector efficiency of 89.73 % compared to asphalt, sand, and sand with water-filled tubes. Similarly, Cuce et al. (Cuce et al., 2022) concluded that there is no significant difference between the performance of an SCPP equipped with natural sand or gravel as the TES material. Their steady-state numerical simulation showed that both materials yield an output power of 41.636 kW for the Manzanares model at a radiation intensity of 800 W/m^2. These studies highlight the importance of TES material selection and optimization in enhancing SCPP performance. However, they also indicate the need for more comprehensive analyses of material properties and their dynamic interactions under varying operational conditions.

Optimization methods, including the Response Surface Methodology (RSM), have been extensively applied to enhance the performance of various solar energy systems. A comprehensive review by Banos et al. (Banos et al., 2011) highlights the state-of-the-art computational optimization techniques in renewable and sustainable energy. It emphasizes their role in improving system efficiency, reducing costs, and addressing design challenges. The study showed the importance of optimization in achieving reliable and cost-effective solar energy solutions. Similarly, Al-Shahri et al. (Al-Shahri et al., 2021) provided a detailed review of intelligent optimization methods used in solar energy systems, focusing on objectives such as minimizing investment, operation, and maintenance costs while enhancing system reliability and reducing emissions. Their work demonstrates the versatility of optimization techniques in addressing complex design and operational challenges across diverse solar technologies. Furthermore, optimization has been critical in improving the thermal performance of solar energy devices. A recent review by Afzal et al. (Afzal et al., 2023) explored the application of meta-heuristic algorithms in optimizing solar thermal systems to show their effectiveness in solving non-linear and multi-objective optimization problems.

As a matter of fact, these recent advancements in SCPP optimization have been significantly enhanced through the application of CFD, RSM, and machine learning techniques. For instance, studies such as Murena et al. (Murena et al., 2022) and Cuce et al. (Cuce et al., 2021) have utilized CFD to analyze fluid dynamic performances and the impact of ground slope on SCPP efficiency. These advancements have also provided validated models for urban integration (Mebarki et al., 2022b). Additionally, machine learning approaches have been employed to optimize SCPP performance, as demonstrated by Salari et al. (Salari et al., 2023) and Ulucak et al. (Ulucak et al., 2021) who developed predictive models for combined solar chimney-photovoltaic thermal systems. Furthermore, Azad et al. (Azad et al., 2021) applied neural networks for multi-objective optimization to highlight the potential of AI-driven methods in enhancing SCPP efficiency for power generation and water desalination. These studies collectively illustrate the widespread adoption and success of optimization methods in advancing solar energy technologies and provide a strong foundation for their application in SCPPs.

However, these studies rarely account for the dynamic, non-linear interactions between TES material properties and SCPP performance under varying meteorological conditions. Furthermore, few have employed advanced numerical techniques like CFD to simulate the heat transfer processes within the system, coupled with optimization methodologies to identify optimal TES configurations. Addressing these gaps is essential to advancing the design and operational efficiency of SCPPs.

This research aims to address these gaps by integrating advanced CFD simulations with RSM to analyze and optimize the effects of ground TES material properties on SCPP performance. The study evaluates key material parameters, including thermal conductivity, specific heat capacity, and density, under actual meteorological conditions in Aswan, Egypt. This region offers an ideal setting for studying SCPPs due to its high solar irradiance and arid climate. The combined CFD-RSM approach enables the detailed modeling of heat transfer processes and their interactions with performance metrics, such as temperature rise, updraft velocity, and collector efficiency. By developing regression models and optimization frameworks, the study aims to identify optimal TES configurations that maximize energy output and minimize fluctuations.

The significance of this research lies in its novel integration of CFD and RSM to support the ongoing research on TES material interactions within SCPPs. Unlike previous studies, this work systematically evaluates the combined effects of multiple material properties under realistic conditions. Our goal is to offer reliable intuitions for optimizing TES configurations. The results of this study are expected to benefit researchers and engineers by providing a validated framework for designing efficient and reliable SCPPs, particularly in regions with high solar potential. Furthermore, the optimization methodologies developed in this study can be adapted to other renewable energy systems that rely on thermal storage, hence contributing to the broader field of sustainable energy technologies.

2. Materials and method

2.1. Physical structure and geometrical design

The SCPP used in this study is modeled based on the geometric specifications of the Manzanares prototype (Cuce et al., 2020), a benchmark system widely referenced in solar chimney research. The SCPP consists of three primary components: the collector, the chimney, and the turbine. The collector, with a mean radius of 122 m, is a transparent or semi-transparent canopy that captures solar radiation, transferring heat to the ground beneath. This heat exchange increases air temperature, creating buoyancy forces that drive airflow toward the centrally located chimney.

The chimney, which is 194.6 m tall with a radius of 5.08 m, amplifies the upward airflow by creating a pressure gradient between its base and the atmosphere at its top. The height and diameter of the chimney play a crucial role in determining the velocity and volume of the airflow. At the chimney's base, a turbine harnesses the kinetic energy of the airflow, converting it into mechanical energy and subsequently into electricity via a generator.

The canopy height, averaging 1.85 m, governs the thermal and aerodynamic behavior of the air beneath the collector, influencing the system's overall performance. Full dimensions of the SCPP are given in Table 1. Fig. 1 provides a schematic representation of the SCPP, showing the interaction of these components and their geometric layout. This configuration is critical for understanding the interaction between system geometry and performance.

2.2. Numerical modeling of SCPP

The numerical simulation of SCPP involves modeling the buoyancy-induced airflow driven by solar heating, which is inherently turbulent due to the high Reynolds number of the flow. Additionally, solar radiation plays a significant role in the system's thermal dynamics, as solar energy is the primary driver of airflow and heat transfer processes. To simplify the numerical solution, we applied these assumptions:

- Airflow within the domain is treated as incompressible, steady, and turbulent.
- The chimney wall is assumed to be adiabatic, meaning heat transfer between the chimney and the ambient air is neglected.
- Thermal inertia is considered only for the TES layer, while temporal changes in fluid mass inertia are disregarded.
- The Boussinesq approximation (Spiegel and Veronis, 1960) is employed, assuming a small temperature difference within the collection system and through the solar chimney (see Section 2.2.1).
- The influence of ambient wind entering the solar collector and mixing with the heated air is excluded.
- The turbine efficiency is assumed to be fixed at 80 %, a value consistent with typical efficiencies reported for axial flow turbines in SCPPs (Daabo et al., 2017; Balijepalli et al., 2018; Rabehi et al., 2018). This value was chosen in this study and previous studies based on empirical data and computational studies that demonstrate the performance of axial flow turbines under similar operating conditions. While the turbine efficiency was not the primary focus of this study, it was incorporated into the power output calculations to ensure a realistic representation of the system's energy conversion process. The power output was derived from the updraft velocity, airflow characteristics, and chimney dimensions. It is used as a key variable for grid sensitivity to ensure grid conversion (see Section 2.2.3).
- The absorptivity and transmittance of the glass cover are set to 0.1 and 0.9, respectively.

Table 1
Geometric specifications of the Manzanares power plant (Cuce et al., 2020).

Mean collector Radius (R_{coll})	122 m
Tower height (H_{ch})	194.6 m
Tower radius (R_{ch})	5.08 m
Average canopy height (H_c)	1.85 m

The simulations were performed in this study using the commercial solver ANSYS Fluent software. Following the numerical setup detailed in (Hachicha et al., 2024), the following sections provide the computational methodology, including the governing equations, turbulence and radiation models, and the computational domain and procedures.

2.2.1. Governing equations

The conservation equations for mass, momentum, and energy govern the flow model of the SCPP. These are solved using ANSYS software, applying appropriate boundary conditions. The steady-state form of the governing equations is expressed in tensor form as follows:

Continuity equation:

$$\nabla(\rho\cdot\vec{v}) = 0 \tag{1}$$

This equation ensures that mass is conserved within the flow domain, meaning that the mass flow rate entering and leaving a control volume remains balanced. In the context of the SCPP, it accounts for the airflow through the collector and chimney, driven by buoyancy effects.

Momentum equation:

$$\nabla\cdot(\rho\cdot\vec{v}\cdot\vec{v}) = -\nabla p + \nabla\cdot\left(\mu\left[(\nabla\vec{v}+\nabla\vec{v}^{T}) - \frac{2}{3}\nabla\cdot\vec{v}|I\right]\right) + \rho\vec{g} \tag{2}$$

This equation describes the balance of forces acting on the air within the SCPP, including pressure gradients, viscous forces, and buoyancy effects. The term ρg represents the buoyancy force due to temperature differences, which drives airflow inside the chimney. Since the flow inside the SCPP exhibits strong buoyancy-induced turbulence, the turbulence model accounts for the additional stresses within the system.

Energy equation:

$$\nabla\left[\rho\vec{v}\left(e+\frac{|\vec{v}|}{2}\right)\right] = \nabla\left(k_{\text{eff}}\nabla T - \sum_j h\vec{J_j} + \bar{\tau}_{\text{eff}}\bullet\vec{v}\right) + S_h \tag{3}$$

where k_{eff} is the effective thermal conductivity, $\overrightarrow{J_j}$ is the diffusive flux of the j-th species, and S_h represents the heat source term attributed to the absorption of solar radiation. I and J can take values 1–3, respectively, representing three mutually perpendicular directions.

This equation represents heat transfer mechanisms, including conduction, convection, and energy exchange due to turbulence. The term $k_{\text{eff}}\nabla T$ accounts for conductive heat transfer, while the convective term $\rho\, v\, e$ represents energy transport due to bulk air movement. The source term S_h accounts for solar radiation absorbed by the ground and air inside the collector.

To accurately capture the buoyancy-driven flow and thermal processes in the SCPP, we employed the Boussinesq approximation (Spiegel and Veronis, 1960), which assumes that variations in density are only significant in the buoyancy term while remaining constant elsewhere. This simplification allows efficient computation without compromising accuracy in low-Mach-number flows. In compressible flow, air density ρ is a function of temperature and pressure, requiring the solution of a fully compressible Navier-Stokes system. However, for natural convection problems, such as those in SCPPs, the variation in density due to pressure is negligible compared to its variation due to temperature. The Boussinesq approximation (Spiegel and Veronis, 1960) assumes that density remains constant in all governing equations except for the buoyancy term in the momentum equation, where it varies linearly with temperature.

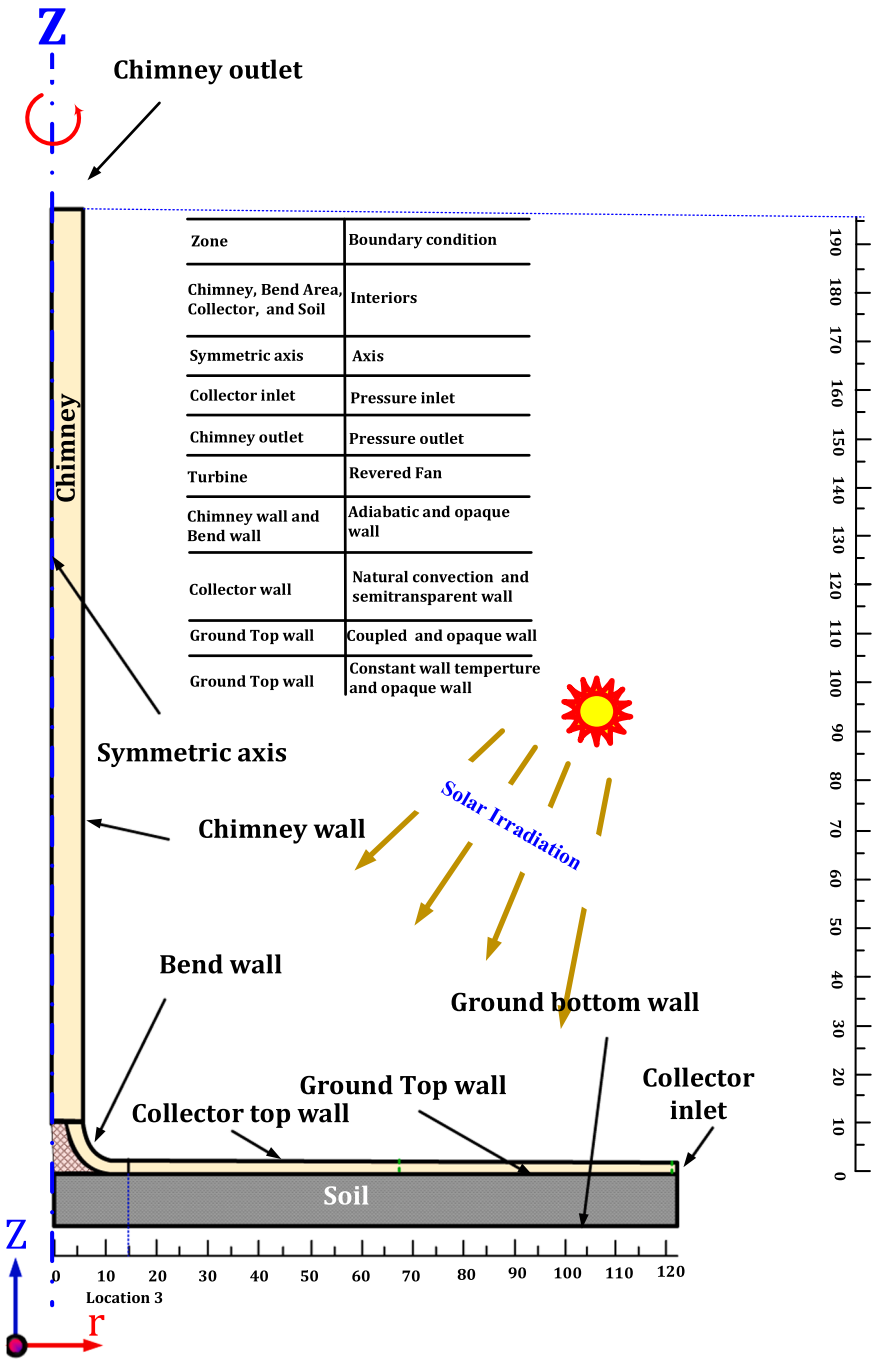


Fig. 1. Schematic diagram of an SCPP model showing the geometry and the boundary conditions.

2.2.2. *Turbulence and radiation models*

The buoyancy-driven flow inside the chimney is a typical turbulent flow since Rayleigh number is calculated to be greater than the critical value of 10^8 (see Hachicha et al. (2024)). For the current simulation, the RNG K-ε turbulence model is employed. This model is chosen because it is particularly effective for capturing strong vortex and swirl effects (Zou and He, 2015). The governing equations for the RNG K-ε turbulence model are presented as follows:

- K-equation

$$\frac{\partial}{\partial x_j}(\rho k \mu_i) = \frac{\partial}{\partial x_j}\left[\left(\mu + \frac{\mu_t}{\sigma_k}\right)\frac{\partial k}{\partial x_j}\right] + G_k + G_b - \rho\varepsilon - Y_M \tag{4}$$

- ε-equation

$$\frac{\partial}{\partial x_j}(\rho \varepsilon \mu_i) = \frac{\partial}{\partial x_j}\left(\left(\mu + \frac{\mu_t}{\sigma_\varepsilon}\right)\frac{\partial \varepsilon}{\partial x_j} + \frac{\varepsilon}{k}(c_1 G_k + c_1 c_3 G_b - c_2 \rho\varepsilon) - R_\varepsilon\right. \tag{5}$$

where ε is its dissipation rate, σ_k and σ_ε are Prandtl numbers related to k and ε, respectively, G_k and G_b are terms representing the generation of turbulent kinetic energy and c_1, c_2 and c_3 are model constants. The symbols μ and μ_t in Eqs. (4) and (5) correspond to the laminar and turbulent viscosity, respectively. The turbulent viscosity μ_t derived from the equation:

$$\mu_t = \rho C_\mu \frac{k^2}{\varepsilon} \tag{6}$$

where C_μ is constant. All constants in the RNG models are chosen based on the numerical setup of Hachicha et al. (Hachicha et al., 2024). All symbols, abbreviations, and nomenclature used in this study are defined in Appendix C.

The discrete ordinates (DO) model is used to parametrize the radiation heat transfer through a semitransparent collector (Ganguli et al., 2021). It converts the radiation transport equation into the transport equation for radiation in spatial coordinates (x,y,z), discretizes the radiation direction change, and solves the radiation transport equation covering the entire space angle in the discrete direction. The DO radiation model and the solar ray tracing algorithm. The software defines the solar beam direction based on the geographic coordinates of the Manzanares pilot plant in Spain.

2.2.3. Computational domain and numerical procedures

As a first step in the computational procedures, a mesh sensitivity analysis was performed to optimize the mesh configuration and ensure that the results were independent of grid size (see Table B1). Given that the computational domain size varied throughout the study, the analysis was conducted for all domains of the solar chimney using the procedures of the grid convergence index (GCI) (Longest and Vinchurkar, 2007; Hefny and Ooka, 2009; Mohamed et al., 2021). In such procedures, five levels of grid refinement were performed and the changes in updraft velocity, temperature rise, collector efficiency, and the power output were evaluated. The results indicated that the fourth refinement level achieved grid independence and further refinement would result in higher computational costs with negligible improvements in accuracy.

The boundary conditions applied to the computational domain are summarized in Table 2. To simulate the flow and thermal behavior accurately, the pressure inlet condition is assigned at the domain's inlet, while a pressure outlet condition is applied at the outlet. The chimney wall is treated as an adiabatic, opaque surface, meaning no heat transfer occurs between the chimney wall and the surrounding environment.

For the collector, a semi-transparent wall boundary condition is applied to simulate the transmission of solar radiation into the system. In this model, the ground will be considered the thermal energy storage layer and is, for analysis purposes, an opaque wall, having the function of absorption and storing heat. A mixed thermal boundary condition has been imposed on both the collector and the ground to capture their respective heat transfer characteristics in the model simulation. These boundary conditions collectively reflect the physical and thermal dynamics of the SCPP system and form the basis for analyzing its performance.

The convective heat transfer coefficient (h) represents the rate of heat exchange between the air inside the collector and the transparent cover. It depends on several factors, including airflow velocity, collector geometry, and ambient conditions. In solar chimney studies, values for h typically range between 5 and 12 W/m^{2}K, depending on experimental and numerical observations. In our study, we adopted a value of h = 9.5 W/m^{2}K based on findings from the literature (Dai et al., 2003; Das and Chandramohan, 2018).

In SCPP systems, the collector is modeled as a semi-transparent surface, which allows sunlight to pass through and transmit energy to the ground. The SIMPLE algorithm was selected to solve the coupling between velocity and pressure fields. A 10^{-6} convergence criterion was adopted to guarantee the results' accuracy and ensure accurate predictions of airflow behavior.

The Boussinesq approximation (Spiegel and Veronis, 1960) was applied to calculate the variation in air density as a function of temperature. The ground zone is modeled as the thermal energy storage layer with specified density, specific heat capacity, and thermal conductivity properties. Simulations are conducted under a range of solar radiation intensity of 200–1000 W/m^2 and a constant ambient temperature of 283–333 K.

The collector's efficiency in a SCPP is pivotal in determining the system's overall performance and energy conversion capability. The collector is the primary interface where solar energy is harnessed, heating the air and initiating the buoyancy-driven airflow required for power generation. It is important to estimate collector performance regarding design optimization and operating practices due to the direct relation of collector performance with the amount of energy that should be converted from solar radiation into usable thermal energy. The useful heat extracted by the collector about the total incident solar energy over the collector area is described mathematically by collector efficiency, η_c. It is expressed as (Yapıcı et al., 2020):

$$\eta_c = \frac{Q}{A_c G} = \frac{\dot{m}\ c_p \Delta T}{A_c G} \tag{8}$$

where $\dot{m}$ is the mass flow in the system

$$\dot{m} = \rho_{ch} A_{ch} v_{ch} \tag{9}$$

2.3. Regression modeling and material optimization

2.3.1. Response Surface Method (RSM)

RSM is commonly used as an optimization approach to examine the input-output correlation for complex systems. It is based on mathematical and statistical methods to estimate and optimize design objectives. Here, it is adopted to generate two different matrices to explore the performance of SCPP under different conditions. This is done to systematically explore critical design parameters and environmental factors affecting selected key performance metrics such as updraft velocity, temperature rise, and collector efficiency. The design of experiments (DOE) incorporates a face-centered design (FCD) methodology, a variant of central composite designs, to effectively capture linear, interaction, and quadratic effects of the variables within the chosen parameter space.

The ranges of parameters considered in the simulations are detailed in Table 3. Thermal conductivity ranges from 0.1 W/m·K up to 5 W/m·K, representing the range from low-conductive sand to highly conductive ceramics. Specific heat capacity ranged from 500 J/kg·K to 5000 J/kg·K, capturing the span of these materials with various capacities that store thermal energy, considering their impacts when the solar radiation is rather low.

Density, ranging from 1000 kg/m^3 to 3000 kg/m^3, simulates lightweight materials such as sand and heavier materials like stones, which play important roles in thermal energy storage. Solar radiation intensities between 200 W/m^2 and 1000 W/m^2 represent conditions from overcast skies to peak sunlight. Ambient temperatures, ranging from

Table 2
Boundary conditions of the numerical setup of SCPP simulations.

Boundary	Conditions	Magnitudes
Collector inlet	Pressure inlet	Zero-gauge pressure
Chimney outlet	Pressure outlet	Zero-gauge pressure
Chimney	Wall (opaque)	Adiabatic
Collector	Wall (semi-transparent)	h = 9.5 W/m^{2}K
Absorber	Wall (opaque)	q = 0 W/m^2
Sidewalls	Wall (opaque)	q = 0 W/m^2

Table 3
Parameter ranges for SCPP simulations.

Parameter	Lower Range	Upper Range	Units
Thermal Conductivity	0.1	5.0	W/m·K
Specific Heat Capacity	500	5000	J/kg·K
Density	1000	3000	kg/m^3
Solar Radiation	200	1000	W/m^2
Ambient Temperature	283	333	K

283 K (10°C) to 333 K (60°C), cover diverse climatic conditions, influencing initial air density and buoyancy-driven flows.

The FCD approach ensures that a sparse number of runs is adopted with excellent parameter space coverage, all under a feasible computational cost. Consequently, the RSM is adopted in the systematic analysis and optimization process, with a two-tier process concerning the performance of Solar SCPP. Five major parameters have been taken into consideration: thermal properties of ground-specific heat capacity, *cp*, thermal conductivity, *k*, and density, ρ; solar radiation and ambient temperature. These were analyzed to construct regression models quantifying the combined effects of these variables on key performance metrics, such as collector efficiency, temperature rise, and updraft velocity. This would have established the fundamental relations among the key variables, such as performance indices, forming the basic model for optimization.

A second RSM matrix was developed with the main ground thermal properties: *cp, k,* and ρ. In this step, the solar radiation and the ambient temperature were taken according to real hourly data measured in Aswan City over three years from July 1, 2021, to June 30, 2024. This was post-processed using MATLAB to give the annual average values; thus, the model will be accurately represented with location-specific environmental conditions.

Accordingly, the optimization was performed using a second DOE matrix, thus giving a concentrated effort in which the effect of ground properties on the SCPP performance could be examined in detail, yielding an optimized configuration that could harness material properties along with site-specific environmental data to realize better efficiency and stability in the system.

2.3.2. MATLAB post-processing and optimization approach

To evaluate the annual performance of SCPP under realistic environmental conditions, MATLAB simulations were employed for post-processing and optimization. These simulations utilized regression models derived from CFD results to estimate key performance metrics—updraft velocity, temperature rise, and collector efficiency—based on meteorological data from Aswan, Egypt (July 2021 – June 2024). The MATLAB framework consists of four primary stages: data preprocessing, regression model application, performance simulation, and optimization of ground material properties.

1. Data Input and Preprocessing

- Hourly solar radiation and ambient temperature data were imported into MATLAB from meteorological records.
- CFD-derived performance metrics for different material properties were structured into a dataset for regression analysis.

2. Regression Model Development

- RSM was used to establish polynomial regression equations correlating updraft velocity, temperature rise, and collector efficiency with ground thermal properties (thermal conductivity, specific heat capacity, and density), solar radiation, and ambient temperature.
- The accuracy of these equations was validated by comparing the predicted results with the CFD simulations.

3. Performance Simulation

- The validated regression models were applied to the meteorological dataset to compute hourly variations in updraft velocity, temperature rise, and collector efficiency.
- These calculations enabled the assessment of the annual system performance trends and to show periods of peak and reduced efficiency.

4. Optimization of Ground Material Properties

- A secondary RSM optimization was performed to focus on determining the optimal combination of thermal conductivity, specific heat, and density under real meteorological conditions.
- The optimization objective was to maximize collector efficiency while ensuring stable performance across different solar radiation levels.

To simplify the analysis while maintaining accuracy, the following assumptions were made:

- The regression equations derived from CFD simulations are valid across the range of environmental conditions encountered in Aswan.
- Heat transfer within the SCPP is primarily governed by radiation and convection, with conduction effects being limited to ground material properties.
- Air properties (e.g., density, specific heat) are assumed to be constant within each time step but vary with temperature in the CFD-derived regression models.
- The solar radiation input follows measured values, assuming no significant shading or obstruction effects.
- The optimization process focuses on material property selection rather than structural modifications to the SCPP.

To clarify the computational steps, a flowchart summarizing the MATLAB workflow for post-processing and optimization is given in Figure D.1 in Appendix D.

3. Results and discussion

3.1. Validation of the present study

The computational model was validated by comparing the simulated results with experimental data from Haaf et al. (Haaf, 1984) and Guo et al. (Hua Guo et al., 2014). The key parameter for validation was the updraft velocity ($V_{updraft}$) under varying solar heat flux (G_h), which was compared against the experimental values from Haaf et al. (Haaf, 1984) and Guo et al. (Hua Guo et al., 2014), as well as the current model's predictions. Fig. 2 represents the comparison, which reflected that the results from the CFD model agreed with the experimental data; thus, the reliability and accuracy of predictions could be established. It should be underlined that the validation case was also treated as a base case for further analysis and comparisons in the present study.

The numerical model used for validation is the same as the one applied in the subsequent simulations and parametric analysis. All governing equations, boundary conditions, turbulence and radiation models, and numerical methods remained unchanged. Only the input parameters, such as ground material properties, solar radiation, and ambient temperature, were adjusted for optimization purposes while maintaining the validated computational framework.

3.2. Soil thermal properties optimization

Most studies on the characteristic parameters of solar chimneys adopt the single-factor analysis method. Its limitation is that it is difficult to reflect the continuous changes of the target response under the influence of the interaction between factors. In contrast, this study uses response surface analysis to model complex interaction relationships.

A computational approach was developed to evaluate the annual performance of a solar chimney system in Aswan, Egypt, focusing on three primary performance metrics: updraft velocity, temperature rise, and collector efficiency. The study utilized meteorological data from NASA specific to Aswan, covering the period from July 1, 2020, to June 30, 2024. This dataset included hourly values of solar radiation and ambient temperature, filtered to include only conditions with solar radiation levels above 200 W/m^2, thereby ensuring relevance to periods of substantial solar activity.

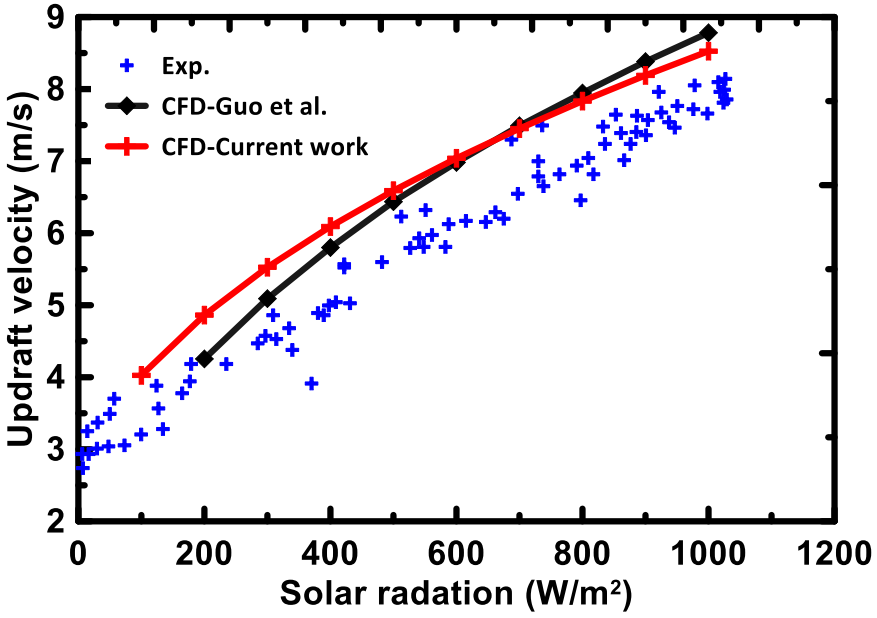


Fig. 2. Validation of CFD Model Updraft Velocity with Experimental Data (Haaf, 1984) and CFD from literature (Hua Guo et al., 2014).

To assess the impact of material configurations within the solar chimney system, an initial design matrix was established using the RSM design matrix (Appendix A, Table A.1), incorporating solar radiation, ambient temperature, and ground thermal properties [thermal conductivity (A), specific heat (B), and density (C)]. RSM was used to derive three regression models to estimate updraft velocity, temperature rise, and collector efficiency under varied material properties and environmental conditions specific to Aswan. These models included each factor's main effects, interaction terms, and quadratic terms, capturing the complex dependencies influencing each performance metric, as shown in Appendix A, Table A.1.

The initial RSM-based regression models, which accounted for solar radiation, ambient temperature, and material properties, were applied to the NASA dataset for each parameter set, calculating system performance hourly. These hourly calculations of updraft velocity, temperature rise, and collector efficiency were then averaged to provide representative annual values for each parameter configuration.

An updated design matrix was constructed to refine the analysis, focusing solely on ground thermal properties, thermal conductivity, specific heat, and density as primary variables (A, B, C) for a second RSM evaluation (Appendix A, Table A.2). This matrix represented the parameter space under the annual meteorological conditions specific to Aswan and enabled a focused regression analysis on the influence of the ground's thermal properties. The final RSM regression models were then applied to this updated matrix, generating results that clarified the impact of Aswan's ground thermal properties on the solar chimney's annual performance metrics. The results of the variance analysis of the regression model in terms of actual factors are shown in Table 4.

The results show the effects of varying material properties and environmental conditions on the performance of a solar chimney system in Aswan, Egypt. Each configuration of thermal conductivity, specific heat, and density, representing different ground material properties, yielded unique values for updraft velocity, temperature rise, and collector efficiency. The values were averaged across all hours in the period analyzed to comprehensively assess the solar chimney's annual performance under Aswan's climatic conditions. Response surface analysis of thermal properties of ground material, ambient temperature, and solar radiation in the effect of updraft velocity, temperature raise, and collector efficiency in three-dimensional surface are shown in Fig. 3.

Fig. 3 shows the interactions between key factors, including thermal conductivity (A), specific heat (B), density (C), solar radiation (D), and ambient temperature (E), and their effects on the performance metrics of Solar Chimney Power Plants (SCPP): updraft velocity, temperature rise, and collector efficiency. These interactions are extremely useful in deducing how material properties and environmental conditions interact to influence the performance of a system. The interaction between thermal conductivity and specific heat (AB) in updraft velocity demonstrates that the retention of heat is improved with higher specific heat. On the other hand, higher thermal conductivity may enhance heat's dissipation and reduce its effect. The interaction between solar

Table 4
Regression equations were derived using the RSM to evaluate the effects of ground properties, solar radiation, and ambient temperature on collector efficiency, temperature rise, and updraft velocity in the solar chimney power plant.

	Updraft Velocity	Temperature rise	Collector efficiency
Intercept	−25.5533	508.2255	−370.721
Thermal Conductivity	−0.10767	0.733259	6.70078
Specific heat	0.000025	−0.00023	0.000413
Density	0.000091	−0.00086	0.00152
Solar radiation	0.025687	0.016745	0.033475
Ambient Temperature	−0.02878	−2.98706	2.40813
Thermal Conductivity * Specific heat	9.99E−21	1.17E−17	−1.5E−09
Thermal Conductivity * Density	−5.4E−19	2.83E−17	−3.5E−09
Thermal Conductivity * Solar radiation	−4.4E−05	−0.0003	0.001652
Thermal Conductivity * Ambient Temperature	0.00016	−0.00337	−0.03126
Specific heat * Density	−1.6E−22	3.24E−20	−3.8E−12
Specific heat * Solar radiation	3.4E−22	8.14E−20	−9.4E−12
Specific heat * Ambient Temperature	3.76E−21	1.26E−18	−1.5E−10
Density * Solar radiation	2.38E−21	1.77E−19	−2.1E−11
Density * Ambient Temperature	−5E−20	2.73E−18	−3.4E−10
Solar radiation * Ambient Temperature	−6.3E−05	1.34E−06	−0.00007
Thermal Conductivity^2	−0.00088	0.034842	0.00005
Specific heat^2	−4.5E−09	4.23E−08	−7.5E−08
Density^2	−2.3E−08	2.14E−07	−3.8E−07
Solar radiation^2	−1.7E−06	−3.4E−06	−6.4E−06
Ambient Temperature^2	0.000421	0.004391	−0.00357

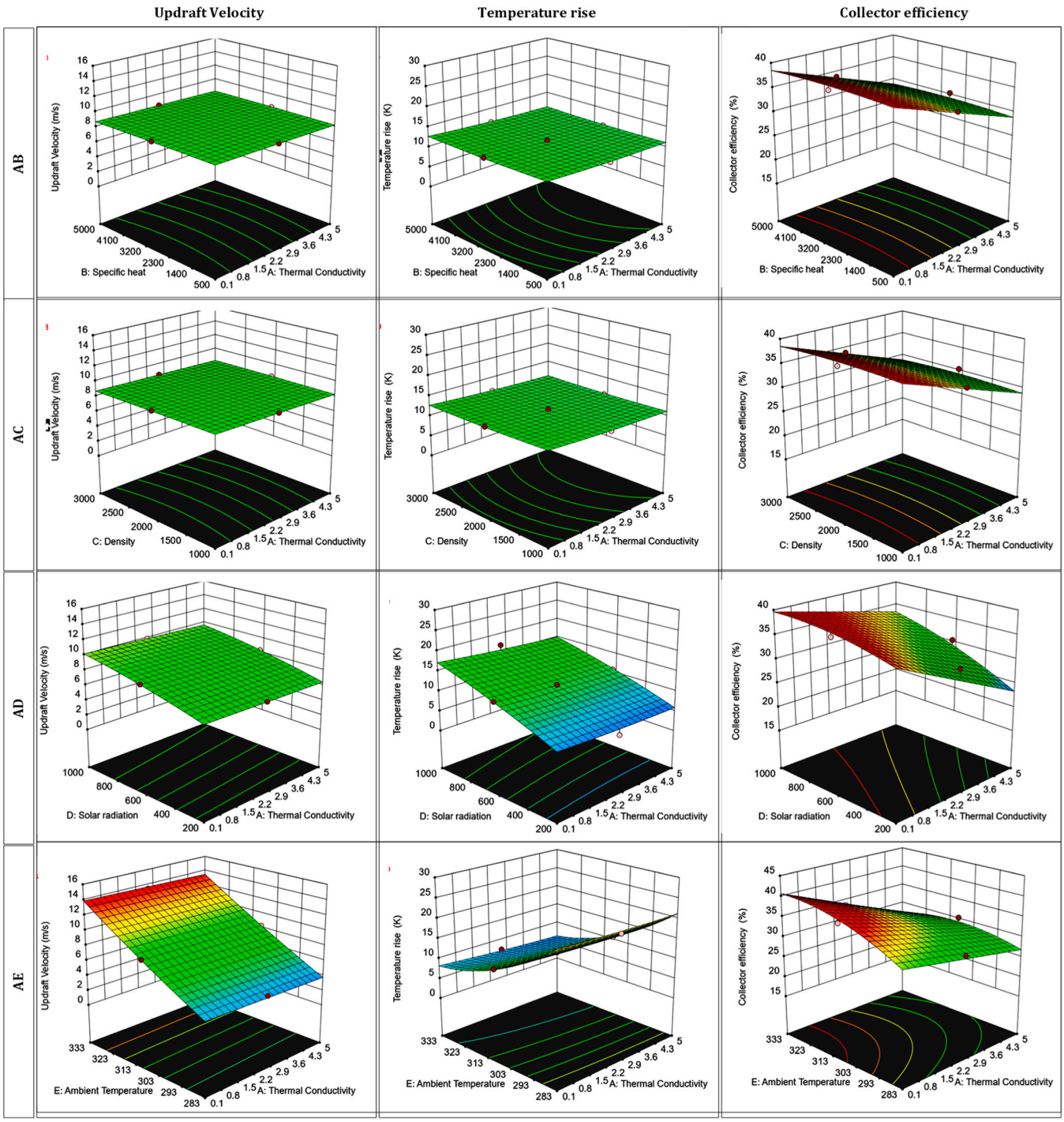


Fig. 3. Response surface for factors interact on (a) updraft velocity, (b) temperature rise, and (c) collector efficiency.

radiation and thermal conductivity (AD) shows that higher solar radiation enhances the buoyant forces acting on air to create flow; thermal conductivity may amplify or reduce this effect depending on material properties. The interaction between thermal conductivity and ambient temperature A-E illustrates that as the ambient temperature increases, the thermal gradient decreases, decreasing airflow velocity within the chimney.

For the temperature rise, the relationship between the product of thermal conductivity and specific heat, AB, yields, and materials of higher specific heat increases the heat retained, hence having a higher rise in temperature. The increased thermal conductivity reduces this advantage by facilitating loss of heat. Solar radiation, AD, now becomes the most significant factor causing the rise in temperature, the influence of which is moderated by the heat retention property of the material. The interaction between solar radiation and ambient temperature, DE, underlines how higher ambient temperatures reduce net thermal gain with emphasis from environmental conditions.

About collector efficiency, thermal conductivity and specific heat interaction AB shows that the right balancing of the properties is critical. High specific heat means improved heat retention while low thermal conductivity means very low losses. Solar radiation strongly influences the collector's efficiency, while increased solar input will increase performance when material properties are optimized. Also, the interaction between thermal conductivity and ambient temperature shows that

higher ambient temperatures decrease the efficiency by reducing the thermal gradient, hence reinforcing again the need for good management of heat losses.

Results also highlight the significance of material thermal properties and environmental conditions in determining system performance. Optimized configurations of thermal conductivity and density, combined with high solar radiation, lead to substantial temperature increases within the system, as shown in Fig. 3. This finding emphasizes the importance of selecting materials with favorable thermal properties, particularly in climates like Aswan's, where the system's ability to absorb and retain heat can be maximized. The sensitivity of temperature rise to both ground material properties and solar radiation suggests that careful selection of these factors can significantly improve the thermal efficiency of the solar chimney. These results underline the complexity of optimizing SCPP performance and the critical role of materials and environmental conditions in enhancing energy conversion efficiency.

The results from the MATLAB simulations shown in Fig. 4 provide detailed hourly variations of the SCPP performance metrics, including updraft velocity, temperature rise, and collector efficiency, over the analyzed period in Aswan City from July 2021 to June 2024. The updraft velocity displayed a clear diurnal cycle, with maximum values observed during midday hours when solar radiation peaks and minimal values at night or during periods of low solar input. Similarly, the temperature rises within the collector system strongly correlated with solar radiation intensity, reaching higher values during the day, and decreasing overnight. Collector efficiency followed the same pattern, achieving its highest values under peak solar conditions while dropping during low-radiation periods. These results show the dependency of SCPP performance on solar radiation and ambient temperature, showcasing the cyclic nature of energy generation in such systems. Hence, optimizing material properties and system design is important to enhance performance during peak operational periods and maintain stability during off-peak times.

While the results of this study show the dependency of SCPP performance on solar radiation and ambient temperature, it is important to note that contradictory findings sometimes are presented in literature, particularly regarding the impact of ambient temperature. For instance, Guo et al. (Hua Guo et al., 2014) reported that ambient temperature variations have little effect on air temperature rise, despite their significant influence on airflow velocity. They also found that the power output of SCPPs within the common diurnal temperature range is relatively insensitive to ambient temperature changes. In contrast, our study demonstrates that ambient temperature plays a dual role in SCPP performance: it directly affects the thermal gradient driving buoyancy-induced airflow and indirectly influences heat retention and dissipation within the system. Specifically, higher ambient temperatures reduce the thermal gradient, leading to lower updraft velocities and collector efficiency, as observed in the current results. On the other hand, solar radiation remains the dominant factor, driving buoyancy-induced airflow through radiation interaction processes (Salim et al., 2022), which heat the ground and the air beneath the collector. Our findings differ from previous works by systematically evaluating the combined effects of ambient temperature and solar radiation under realistic meteorological conditions, using advanced CFD-RSM techniques. The results emphasize that while ambient temperature has a measurable impact on SCPP performance, its influence is secondary to solar radiation, which is the primary driver of system efficiency. This finding may explain some of the contradictions in the literature and provides a more comprehensive framework for optimizing SCPP performance under varying environmental conditions.

Collector efficiency was particularly responsive to variations in thermal conductivity and ambient temperature. Higher collector efficiency was observed with increased thermal conductivity, while extreme ambient temperatures showed diminishing returns, as indicated by the quadratic terms in the regression model. This suggests that while increased thermal conductivity benefits overall efficiency, optimal performance occurs within a specific temperature range. The results indicate that enhancing collector efficiency in solar chimney systems may depend on careful consideration of material selection, as the right balance of thermal properties and ambient temperature can significantly impact the system's efficiency.

Fig. 5 Show the main effect plots results of the second design matrix (Appendix A, Table A.2), illustrating the influence of ground thermal properties, thermal conductivity, specific heat capacity, and density on

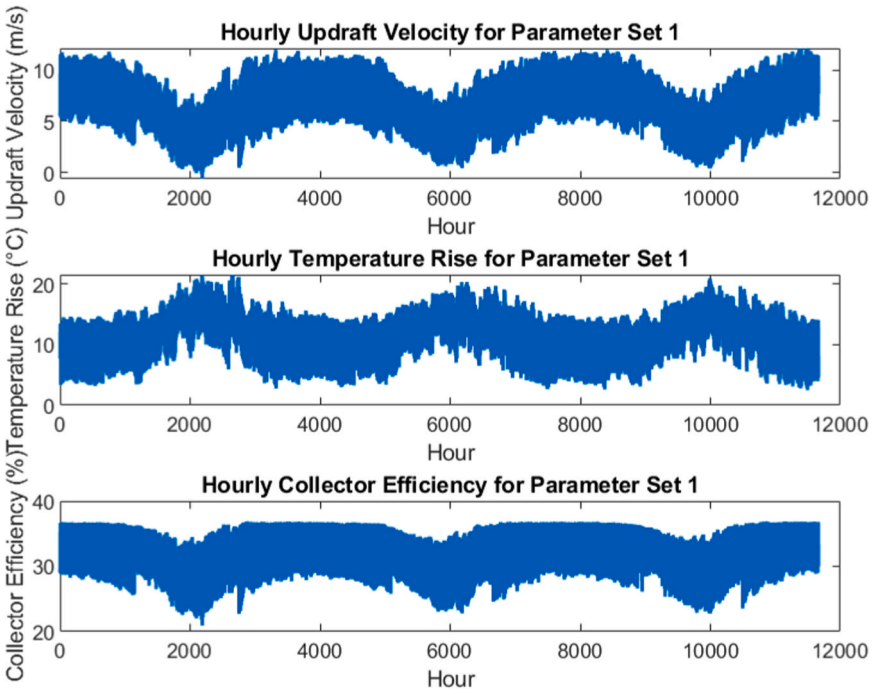


Fig. 4. Hourly variations of updraft velocity, temperature rise, and collector efficiency for SCPP in Aswan City, simulated over three years using MATLAB. The plots highlight the diurnal dependency of performance metrics on solar radiation and ambient.

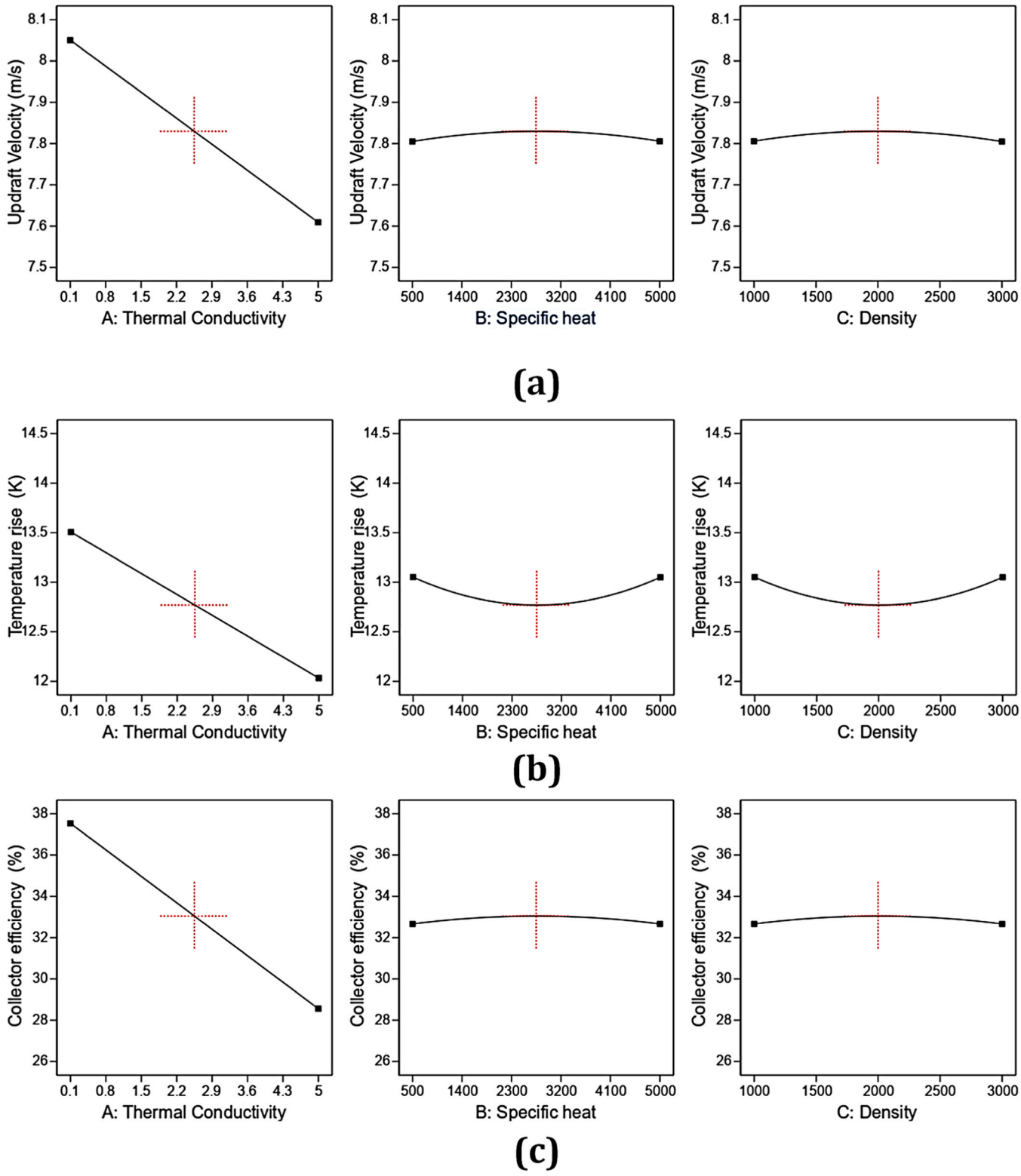


Fig. 5. Main Effects Plots: Influence of Ground Thermal Properties (Thermal Conductivity, Specific Heat Capacity, and Density) on SCPP Performance Metrics: (a) Updraft Velocity, (b) Temperature Rise, and (c) Collector Efficiency.

the key performance indicators of an SCPP: updraft velocity, temperature rise, and collector efficiency. For updraft velocity Fig. 5(a), thermal conductivity shows a marked negative correlation, with values decreasing from 8.1 m/s to 7.5 m/s as thermal conductivity increases from 0.1 W/m·K to 5 W/m·K. This demonstrates the significant impact of heat dissipation on airflow dynamics, where higher thermal conductivity reduces the buoyant forces driving airflow. In contrast, specific heat and density exhibit minimal variation, with updraft velocity remaining steady at approximately 7.8 m/s, indicating a less pronounced effect on airflow within the chimney. For temperature rise Fig. 5(b), the effect of thermal conductivity is similarly negative, with the temperature rise dropping from 14.5 K to 12.5 K as thermal

conductivity increases. Specific heat and density display a concave relationship, with the temperature rising at around 14 K for intermediate values of specific heat (approximately 2500 J/kg·K) and density (2000 kg/m^3). These findings suggest that while thermal conductivity predominantly affects heat retention, specific heat, and density are secondary in moderating thermal storage efficiency.

For collector efficiency Fig. 5(c), thermal conductivity again exhibits a decreasing trend, with efficiency falling from 38 % to 28 % as thermal conductivity increases. This highlights the negative impact of higher heat dissipation rates on system performance. Specific heat and density demonstrate a modest improvement in collector efficiency, peaking at 37 % for intermediate values. This indicates that balanced thermal properties can improve energy conversion efficiency by enhancing heat retention and minimizing losses.

Key observations from the results include the steep decline in updraft velocity (from 8.1 m/s to 7.5 m/s) and temperature rise (from 14.5 K to 12.5 K) with increased thermal conductivity, as well as the peak collector efficiency of 37 % observed for intermediate values of specific heat and density. These results emphasize the importance of selecting ground materials with low thermal conductivity and balanced specific heat and density to optimize SCPP performance.

The optimal combination of ground material properties for maximizing the average collector efficiency of the Solar Chimney Power Plant (SCPP) was determined using a two-step process based on the RSM and optimization techniques implemented in MATLAB. The analysis identified thermal conductivity (0.1 W/m·K), specific heat capacity (2750 J/kg·K), and density (2000 kg/m^3) as the optimal combination. This configuration minimized heat losses, maximized energy retention, and ensured efficient energy transfer, leading to Aswan's highest collector efficiency under specific environmental conditions. The case that was optimized for the same value of 1000 W/m^2 is given in Fig. 6 below: temperature contours (a) are quite regular with maximum heat accumulation just below the base of the chimney, thus assisting buoyancy forces, while the velocity contours in b are smooth and at maximum value inside the throat of the chimney, which reflects good energy conversion and performance of the system.

Fig. 7 compares the key performance indices between the base and optimum cases. In all solar radiation ranges, the updraft velocity, temperature increase, collector efficiency, and power output consistently outperformed the base case. The optimum case was improved updraft velocity, ranging from 4.62 % at the lowest solar radiation levels to 4.22 % at the highest radiation levels, as clear in Fig. 7(a). As shown in Fig. 7(b), the temperature rise is higher for all radiation levels relative to the optimum case, showing that it retains more heat due to improved material properties. The collector efficiency, Fig. 7(c), is considerably higher for the optimum case; the gap in efficiency increases with the increase in solar radiation; at low radiation level, it improved by 11.15 % and by 6.9 % at the highest solar radiation level. Under optimum conditions, the power output at the lowest solar radiation improved by 17.71 % and 11.05 % at the highest solar radiation as shown in Fig. 7(d). The results confirm that the optimized ground properties are critical, specifically at low solar radiation values.

4. Conclusion

This study investigated the optimization of SCPP performance by carefully selecting ground material properties. Using CFD simulations and the RSM, the study analyzed the effects of thermal conductivity, specific heat capacity, and density on key performance indicators, including updraft velocity, temperature rise, and collector efficiency. The results, based on meteorological data from Aswan, Egypt (July 2021 – June 2024), demonstrated that optimized ground properties significantly enhance SCPP efficiency. Lower thermal conductivity was found to reduce heat dissipation, while intermediate values of specific heat and density improved energy retention and conversion efficiency. Solar radiation emerged as the dominant environmental factor influencing system performance, while ambient temperature played a secondary role by affecting thermal gradients and airflow dynamics.

The findings revealed that the optimal combination of ground material properties for maximizing collector efficiency consisted of a thermal conductivity of 0.1 W/m·K, a specific heat capacity of 2750 J/kg·K, and a density of 2000 kg/m^3 . Increasing thermal conductivity led to a reduction in updraft velocity from 8.1 m/s to 7.5 m/s and a decrease in temperature-rise from 14.5 K to 12.5 K. Higher conductivity in turn enhances heat dissipation and weakens buoyancy-driven airflow. Similarly, collector efficiency declined from 38 % to 28 % with higher thermal conductivity, but an optimal balance of specific heat and density improved efficiency to 37 %. Solar radiation was identified as the most significant factor influencing performance, while ambient temperature had a more limited impact, primarily through its effect on

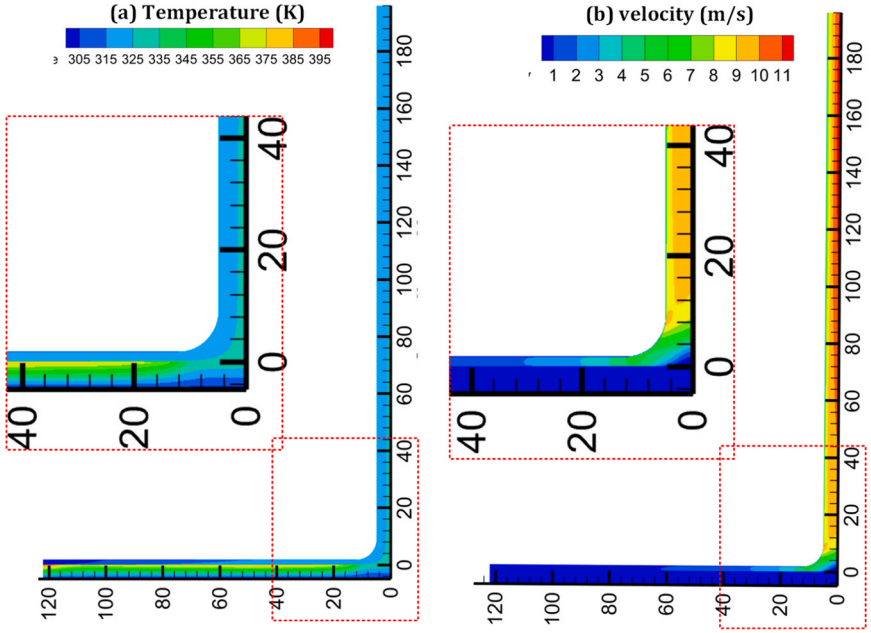


Fig. 6. Contours of (a) temperature and (b) velocity for the optimized case at 1000 w/m^2.

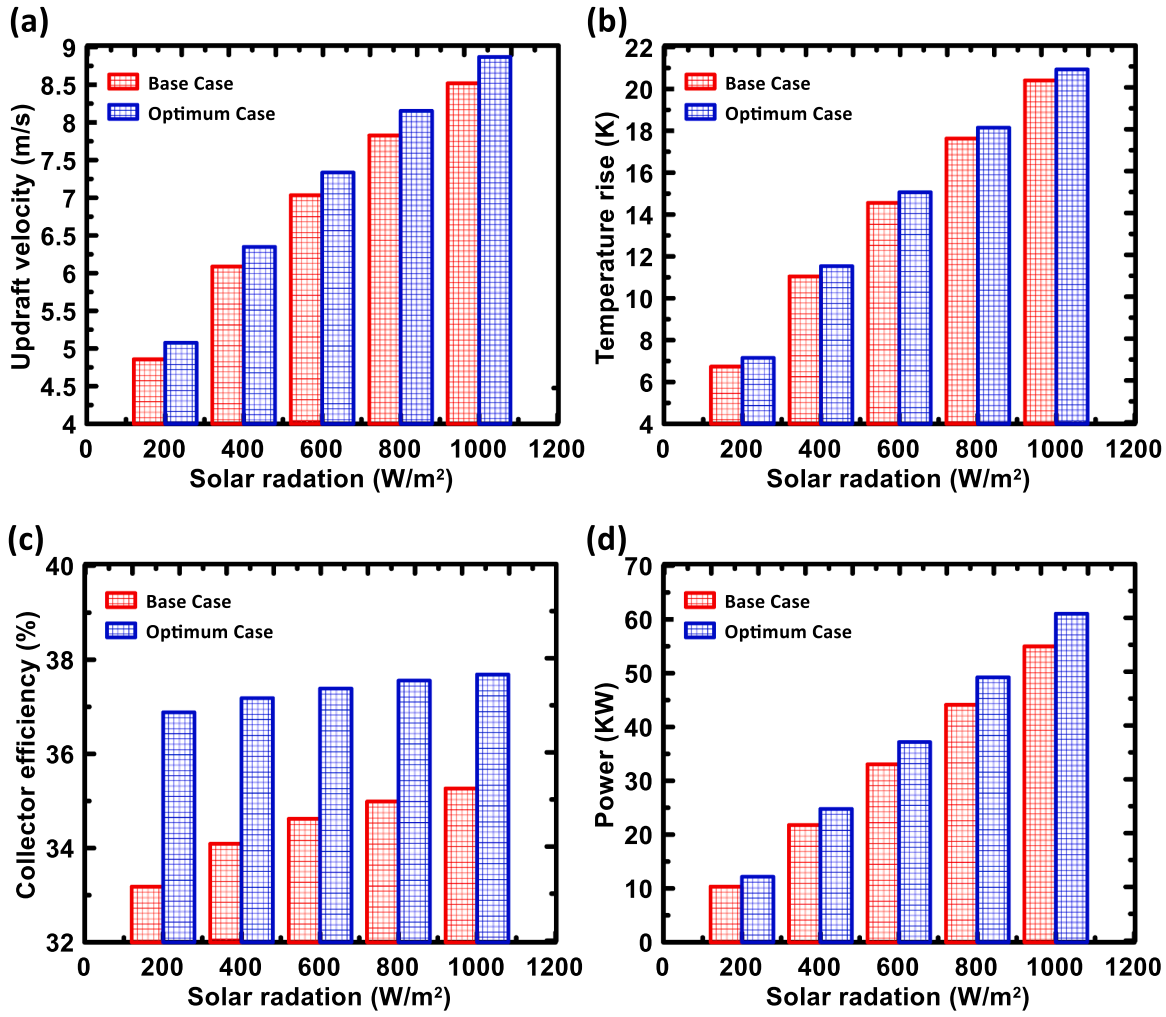


Fig. 7. Comparison between the base case and the optimized case, in (a) updraft velocity, (b) temperature rise, (c) collector efficiency, and (d) power output under varying solar radiation levels.

thermal gradients. Moreover, the optimization of ground material properties resulted in a substantial increase in power output, with improvements of 17.71 % at low solar radiation levels and 11.05 % at high levels.

This study provides a robust framework for optimizing SCPPs in high-solar-potential regions, but further research is needed to enhance system performance and adaptability. Future studies should explore the impact of alternative ground materials with varying thermal properties, investigate the effects of seasonal variations on SCPP efficiency, and examine hybrid configurations that integrate SCPPs with other solar energy technologies. Additionally, research should include the effect of geometric parameters on the optimization of ground material properties, as variations in collector size, chimney height, and other structural elements could influence heat retention, airflow dynamics, and overall system performance. Such advancements could further improve energy output, system stability, and scalability, which would contribute to the broader development of sustainable energy solutions.

CRediT authorship contribution statement

Esmail Mohamed F.C.: Writing – original draft, Methodology, Funding acquisition, Conceptualization. **Salim Mohamed H.:** Writing – original draft, Methodology, Formal analysis, Conceptualization. **Abo-Zahhad Essam M.:** Writing – review & editing, Validation, Methodology, Formal analysis, Conceptualization. **Mistarihi Mahmoud Z.:** Writing – original draft, Methodology, Data curation, Conceptualization. **Hachicha Ahmed Amine:** Writing – original draft, Methodology, Formal analysis, Conceptualization.

Declaration of Competing Interest

The authors declare that they have no known competing financial interests or personal relationships that could have appeared to influence the work reported in this paper.

Appendix A. Design matrices for RSM and experimental analysis

Table A.1
The initial design matrix used for RSM incorporates ground properties (thermal conductivity, specific heat, and density), solar radiation, and ambient

			Factor 1	Factor 2	Factor 3	Factor 4	Factor 5	Response 1	Response 2	Response 3
Std	Group	Run	A: K	B: Cp	C: ρ	D: G	E: T_a	$V_{Updraft}$	ΔT	η_c
			W/m.K	J/kg.K	Kg/m^3	W/m^2	K	m/s	K	%
1	4	29	0.1	500	1000	200	283	1.56	17.07	27.06
2	4	17	0.1	5000	1000	200	283	1.56	17.07	27.06
3	4	18	0.1	500	3000	200	283	1.56	17.07	27.06
4	4	19	0.1	5000	3000	200	283	1.56	17.07	27.06
5	4	16	0.1	500	1000	1000	283	6.22	27.46	34.68
6	4	28	0.1	5000	1000	1000	283	6.22	27.46	34.68
7	4	22	0.1	500	3000	1000	283	6.22	27.46	34.68
8	4	20	0.1	5000	3000	1000	283	6.22	27.46	34.68
9	4	14	0.1	500	1000	200	333	12.49	3.09	39.11
10	4	27	0.1	5000	1000	200	333	12.49	3.09	39.11
11	4	15	0.1	500	3000	200	333	12.49	3.09	39.11
12	4	25	0.1	5000	3000	200	333	12.49	3.09	39.11
13	4	26	0.1	500	1000	1000	333	14.63	13.16	39.03
14	4	23	0.1	5000	1000	1000	333	14.63	13.16	39.03
15	4	24	0.1	500	3000	1000	333	14.63	13.16	39.03
16	4	21	0.1	5000	3000	1000	333	14.63	13.16	39.03
17	7	49	5	500	1000	200	283	1.20	16.80	20.38
18	7	41	5	5000	1000	200	283	1.20	16.80	20.38
19	7	38	5	500	3000	200	283	1.20	16.80	20.38
20	7	40	5	5000	3000	200	283	1.20	16.80	20.38
21	7	45	5	500	1000	1000	283	5.69	25.62	29.59
22	7	37	5	5000	1000	1000	283	5.69	25.62	29.59
23	7	44	5	500	3000	1000	283	5.69	25.62	29.59
24	7	39	5	5000	3000	1000	283	5.69	25.62	29.59
25	7	42	5	500	1000	200	333	12.17	1.61	19.88
26	7	48	5	5000	1000	200	333	12.17	1.61	19.88
27	7	35	5	500	3000	200	333	12.17	1.61	19.88
28	7	46	5	5000	3000	200	333	12.17	1.61	19.88
29	7	50	5	500	1000	1000	333	14.14	10.87	31.17
30	7	43	5	5000	1000	1000	333	14.14	10.87	31.17
31	7	36	5	500	3000	1000	333	14.14	10.87	31.17
32	7	47	5	5000	3000	1000	333	14.14	10.87	31.17
33	1	3	2.55	2750	2000	600	308	8.57	11.72	33.96
34	1	1	2.55	2750	2000	600	308	8.57	11.72	33.96
35	1	2	2.55	2750	2000	600	308	8.57	11.72	33.96
36	5	31	0.1	2750	2000	600	308	8.84	12.74	38.05
37	5	30	0.1	2750	2000	600	308	8.84	12.74	38.05
38	2	5	5	2750	2000	600	308	8.33	10.81	30.42
39	2	4	5	2750	2000	600	308	8.33	10.81	30.42
40	3	10	2.55	500	2000	600	308	8.57	11.72	33.96
41	3	8	2.55	5000	2000	600	308	8.57	11.72	33.96
42	3	11	2.55	2750	1000	600	308	8.57	11.72	33.96
43	3	6	2.55	2750	3000	600	308	8.57	11.72	33.96
44	3	7	2.55	2750	2000	200	308	6.69	4.71	31.96
45	3	9	2.55	2750	2000	1000	308	9.94	17.21	34.68
46	3	12	2.55	2750	2000	600	283	4.27	21.07	30.46
47	3	13	2.55	2750	2000	600	333	13.44	7.43	33.74
48	6	33	2.55	2750	2000	600	308	8.57	11.72	33.96
49	6	32	2.55	2750	2000	600	308	8.57	11.72	33.96
50	6	34	2.55	2750	2000	600	308	8.57	11.72	33.96
51	8	53	2.55	2750	2000	600	308	8.57	11.72	33.96
52	8	51	2.55	2750	2000	600	308	8.57	11.72	33.96
53	8	52	2.55	2750	2000	600	308	8.57	11.72	33.96

Table A.2
Design Matrix 2: Experimental matrix focusing on ground material properties under varying solar radiation and ambient temperature conditions. Hourly solar radiation and ambient temperature data from Aswan

Std	Group	Run	Factor 1 A: K	Factor 2 B: Cp	Factor 3 C: ρ	Response 1 $V_{Updraft}$	Response 2 ΔT	Response 3 η_c
			W/m.K	J /kg1 K1	Kg/m^3	W/m^2	K	m/s
10	1	1	2.55	2750.00	2000.00	7.83	12.72	33.05
11	1	2	2.55	2750.00	2000.00	7.83	12.72	33.05
9	1	3	2.55	2750.00	2000.00	7.83	12.72	33.05
8	2	4	2.55	2750.00	2000.00	7.83	12.72	33.05

(continued on next page)

Table A.2 (*continued*)

Std	Group	Run	Factor 1 A: K	Factor 2 B: Cp	Factor 3 C: ρ	Response 1 $V_{Updraft}$	Response 2 ΔT	Response 3 η_c
5	2	5	2.55	2750.00	2000.00	7.83	12.72	33.05
6	2	6	2.55	2750.00	2000.00	7.83	12.72	33.05
7	2	7	2.55	2750.00	3000.00	7.81	12.94	32.67
23	3	8	2.55	2750.00	1000.00	7.81	12.94	32.67
24	3	9	2.55	5000.00	2000.00	7.81	12.94	32.67
25	3	10	2.55	500.00	2000.00	7.81	12.94	32.67
22	4	11	5.00	2750.00	2000.00	7.61	12.20	28.56
20	4	12	5.00	2750.00	2000.00	7.61	12.20	28.56
21	4	13	0.10	2750.00	2000.00	8.05	13.67	37.53
17	5	14	0.10	2750.00	2000.00	8.05	13.67	37.53
16	5	15	2.55	2750.00	2000.00	7.83	12.72	33.05
18	5	16	2.55	2750.00	2000.00	7.83	12.72	33.05
19	5	17	2.55	2750.00	2000.00	7.83	12.72	33.05
15	6	18	5.00	5000.00	3000.00	7.56	12.62	27.80
14	6	19	5.00	500.00	3000.00	7.56	12.62	27.80
3	7	20	5.00	5000.00	1000.00	7.56	12.62	27.80
1	7	21	5.00	500.00	1000.00	7.56	12.62	27.80
2	7	22	0.10	5000.00	3000.00	8.00	14.10	36.77
4	7	23	0.10	500.00	3000.00	8.00	14.10	36.77
12	8	24	0.10	5000.00	1000.00	8.00	14.10	36.77
13	8	25	0.10	500.00	1000.00	8.00	14.10	36.77

Appendix B. Mesh sensitivity analysis

Table B1
Mesh conversion using GCI approach of mesh refinement

Grid	Element size (m)	No. of Elements	$V_{Updraft}$ (m/s)	ΔT (K)	μ_{col} (%)	P (Kw)
Grid 1	0.50	7302	20.10	34.38	53.62	8.43
Grid 2	0.25	29260	20.35	35.09	54.67	8.51
Grid 3	0.20	45678	20.39	35.22	54.89	8.52
Grid 4	0.15	81579	20.42	35.28	54.99	8.53
Grid 5	0.10	176132	20.41	35.27	54.99	8.53

Appendix C. Nomenclature

Abbreviations

CFD	Computational fluid dynamics
DO	Discrete ordinates
FCD	Face centered design
GCI	Grid convergence index
RSM	Response Surface Methodology
SCPP	Solar Chimney Power Plant
TES	Thermal Energy Storage
DOE	Design of experiments

Symbols

A	Cross sectional area, m^2
cp	heat capacity, J/kg.K
D	Diameter, m
g	Gravity, m/s^2
G	Solar radiation, W/m^2
G_b	Turbulent kinetic energy due to buoyancy, $kg/m.s^3$
G_k	Turbulent kinetic energy due to the velocity gradient, $kg/m.s^3$
H	Height, m
h	Heat transfer coefficient, W/m^2 K
k	Thermal conductivity (W/m.K)
K	Turbulent kinetic energy (m^2/s^2)
$\dot{m}$	Mass flow rate, kg/s
p	Pressure, Pa
Pr	Prandtl number
q	Heat flow, W

R	Radius, m
$v_{updraft}$	Updraft velocity, m/s

Greek symbol

Δp	Pressure difference, Pa
ΔT	Temperature gradient, K
η	Efficiency, %
ρ	Density, kg/m^3
μ	Dynamic viscosity (Pa·s)
ε	Turbulent dissipation rate(m^2/s^3)
σ	Prandtl numbers

Subscripts

c	canopy
coll	Collector
ch	chimney
eff	effective
t	turbulent viscosity
h	heat flux

Appendix D. Flowchart for performance evaluation and optimization

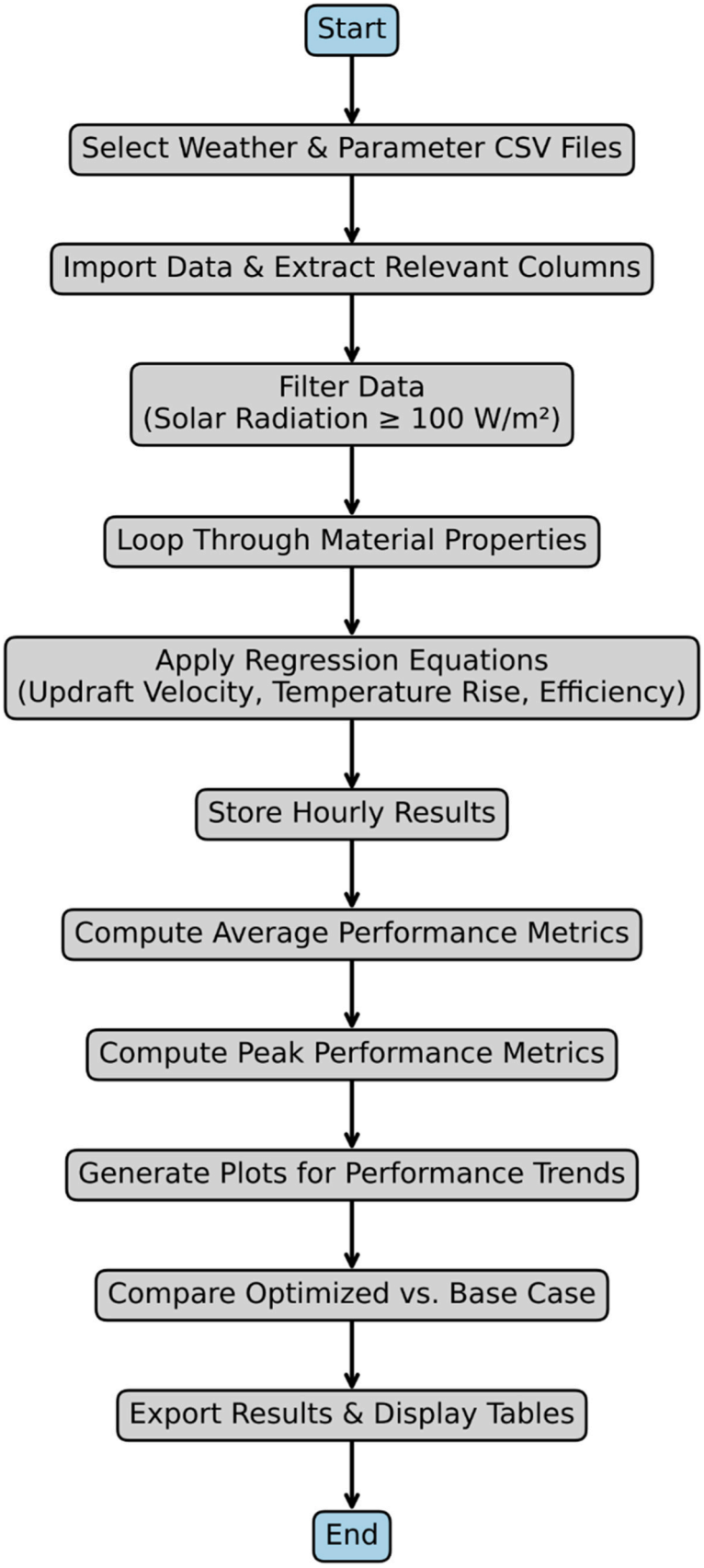


Fig. D.1. Flowchart of MATLAB simulations used for performance evaluation and optimization of ground material properties in the SCPP

Data Availability

No data was used for the research described in the article.

References

Afzal, A., Buradi, A., Jilte, R., Shaik, S., Kaladgi, A.R., Arıcı, M., Lee, C.T., Nižetić, S., 2023. Optimizing the thermal performance of solar energy devices using meta-heuristic algorithms: a critical review. Renew. Sustain. Energy Rev. 173, 112903. https://doi.org/10.1016/j.rser.2022.112903.

Al-Azawiey, S.S., Hassan, S.B., 2016. Heat absorption properties of ground material for solar chimney power plants. Int. J. Energy Prod. Manag. 1 (4), 403–418.

Al-Shahri, O.A., Ismail, F.B., Hannan, M.A., Lipu, M.H., Al-Shetwi, A.Q., Begum, R.A., Al-Muhsen, N.F., Soujeri, E., 2021. Solar photovoltaic energy optimization methods, challenges and issues: a comprehensive review. J. Clean. Prod. 284, 125465. https://doi.org/10.1016/j.jclepro.2020.125465.

Azad, A., Aghaei, E., Jalali, A., Ahmadi, P., 2021. Multi-objective optimization of a solar chimney for power generation and water desalination using neural network. Energy Convers. Manag. 238, 114152. https://doi.org/10.1016/j.enconman.2021.114152.

Balijepalli, R., Chandramohan, V.P., Kirankumar, K., 2018. Optimized design and performance parameters for wind turbine blades of a solar updraft tower (SUT) plant using theories of Schmitz and aerodynamics forces. ISSN 2213-1388 Sustain. Energy Technol. Assess. 30, 192–200. https://doi.org/10.1016/j.seta.2018.10.001.

Banos, R., Manzano-Agugliaro, F., Montoya, F.G., Gil, C., Alcayde, A., Gómez, J., 2011. Optimization methods applied to renewable and sustainable energy: a review. Renew. Sustain. Energy Rev. 15 (4), 1753–1766.

Biswas, N., Kumar Mandal, D., Manna, N.K., Cemal Benim, A., 2023. Novel stair-shaped ground absorber for performance enhancement of solar chimney power plant. Appl. Therm. Eng. 227, 120466. https://doi.org/10.1016/J.APPLTHERMALENG.2023.120466.

Cuce, E., Cuce, P.M., Sen, H., 2020. A thorough performance assessment of solar chimney power plants: case study for Manzanares. Clean. Eng. Technol. 1, 100026. https://doi.org/10.1016/J.CLET.2020.100026.

Cuce, E., Cuce, P.M., Sen, H., Sudhakar, K., Berardi, U., Serencam, U., 2021. Impacts of ground slope on main performance figures of solar chimney power plants: a comprehensive CFD research with experimental validation. Int. J. Photo 2021, 6612222. https://doi.org/10.1155/2021/6612222.

Cuce, E., Saxena, A., Cuce, P.M., Sen, H., Eroglu, H., Selvanathan, S.P., Sudhakar, K., Hasanuzzaman, M., 2022. Performance assessment of solar chimney power plants with natural thermal energy storage materials on ground: CFD analysis with experimental validation. Int. J. Low. -Carbon Technol. 17, 752–759.

Daabo, A.M., Mahmoud, S., Al-Dadah, R.K., Al Jubori, A.M., Ennil, A.B., 2017. Numerical analysis of small scale axial and radial turbines for solar powered Brayton cycle application. Appl. Therm. Eng. 120, 672–693. https://doi.org/10.1016/j.applthermaleng.2017.04.012.

Dai, Y.J., Huang, H.B., Wang, R.Z., 2003. Case study of solar chimney power plants in Northwestern regions of China. Renew. Energy 28 (8), 1295–1304. https://doi.org/10.1016/S0960-1481(02)00227-6.

Das, P., Chandramohan, V.P., 2018. CFD analysis on flow and performance parameters estimation of solar updraft tower (SUT) plant varying its geometrical configurations. Energy Sources, Part A: Recovery, Util. Environ. Eff. 40 (12), 1532–1546. https://doi.org/10.1080/15567036.2018.1476612.

Esmail, M.F.C., Mekhail, T., 2019. Investigations of the instantaneous performance of a solar chimney power plant installed in Aswan using IoT. IET Renew. Power Gener. 13 (12), 2261–2266. https://doi.org/10.1049/iet-rpg.2018.5950.

Esmail, M.F.C., A-Elmagid, W.M., Mekhail, T., Al-Helal, I.M., Shady, M.R., 2021. A numerical comparative study of axial flow turbines for solar chimney power plant. Case Stud. Therm. Eng. 26, 101046. https://doi.org/10.1016/J.CSITE.2021.101046.

Esmail, M.F.C., Khodary, A., Mekhail, T., Hares, E., 2022. Effect of wind speed over the chimney on the updraft velocity of a solar chimney power plant: an experimental study. Case Stud. Therm. Eng. 37. https://doi.org/10.1016/j.csite.2022.102265.

Ganguli, A.A., Deshpande, S.S., Pandit, A.B., 2021. Cfd simulations for performance enhancement of a solar chimney power plant (Scpp) and techno-economic feasibility for a 5 mw scpp in an Indian context. Energies (Basel) 14 (11). https://doi.org/10.3390/en14113342.

Haaf, W., 1984. Solar chimneys: part ii: preliminary test results from the Manzanares pilot plant. Int. J. Sustain. Energy 2 (2), 141–161.

Haaf, W., Friedrich, K., Mayr, G., Schlaich, J., 1983. Solar chimneys part I: principle and construction of the pilot plant in Manzanares. Int. J. Sol. Energy 2 (1), 3–20.

Hachicha, A.A., Abo-Zahhad, E.M., Masmoudi, M., Said, Z., Rahman, S.M.A., 2024. Techno-Economic evaluation and multi-objective optimization of a filter equipped solar chimney system. Renew. Energy 237, 121452. https://doi.org/10.1016/J.RENENE.2024.121452.

Hassan, A., Ali, M., Waqas, A., 2018. Numerical investigation on performance of solar chimney power plant by varying collector slope and chimney diverging angle. Energy 142, 411–425. https://doi.org/10.1016/J.ENERGY.2017.10.047.

Hefny, M.M., Ooka, R., 2009. CFD analysis of pollutant dispersion around buildings: effect of cell geometry. Build. Environ. 44 (8), 1699–1706. https://doi.org/10.1016/j.buildenv.2008.11.010.

Hua Guo, P., Yin Li, J., Wang, Y., 2014. Numerical simulations of solar chimney power plant with radiation model. Renew. Energy 62, 24–30. https://doi.org/10.1016/J.RENENE.2013.06.039.

Hurtado, F.J., Kaiser, A.S., Zamora, B., 2012. Evaluation of the influence of soil thermal inertia on the performance of a solar chimney power plant. Energy 47 (1), 213–224. https://doi.org/10.1016/j.energy.2012.09.040.

Ikhlef, K., Larbi, S., Üçgül, İ., 2022b. Experimental study of different thermal storage system effects on the performance of a small prototype solar chimney power plant. Renew. Energy 200, 516–526. https://doi.org/10.1016/j.renene.2022.09.087.

Ikhlef, K., Larbi, S., Üçgül, İ., 2022a. Experimental study of different thermal storage system effects on the performance of a small prototype solar chimney power plant. Renew. Energy 200, 516–526. https://doi.org/10.1016/j.renene.2022.09.087.

Krumar Mandal, D., Pradhan, S., Chakraborty, R., Barman, A., Biswas, N., 2022. Experimental investigation of a solar chimney power plant and its numerical verification of thermo-physical flow parameters for performance enhancement. Sustain. Energy Technol. Assess. 50. https://doi.org/10.1016/j.seta.2021.101786.

Longest, P.W., Vinchurkar, S., 2007. Effects of mesh style and grid convergence on particle deposition in bifurcating airway models with comparisons to experimental data. Med. Eng. amp; Phys. 29, 350–366. https://doi.org/10.1016/j.medengphy.2006.05.012.

Mamgain, S., Das, S., Sharma, M., Shukla, A.K., 2024. Thermo-economic investigation of the hybrid wind supercharging solar chimney power generation system. Engineering Materials for Efficient Energy Storage and Conversion. IGI Global, pp. 455–488.

Mebarki, Sekhri, A., Assassi, A., Hanafi, A., Marir, B., 2022a. CFD analysis of solar chimney power plant: finding a relationship between model minimization and its performance for use in urban areas. Energy Rep. 8, 500–513. https://doi.org/10.1016/j.egyr.2021.12.008.

Mebarki, A., Sekhri, A., Assassi, A., Hanafi, A., Marir, B., 2022b. CFD analysis of solar chimney power plant: finding a relationship between model minimization and its performance for use in urban areas. Energy Rep. 8, 500–513. https://doi.org/10.1016/j.egyr.2022.07.019.

Mohamed, M.A., Maksoud, T., Santos, R.J., Salim, M.H., Esmail, M.F.C., 2021. Ain Shams Eng. J. 12, 2935. https://doi.org/10.1016/j.asej.2021.01.022.

Murena, F., Gaggiano, I., Mele, B., 2022. Fluid dynamic performances of a solar chimney plant: analysis of experimental data and CFD modelling. Energy 249, 123702. https://doi.org/10.1016/j.energy.2022.123702.

Pradhan, S., Chakraborty, R., Mandal, D.K., Barman, A., Bose, P., 2021. Design and performance analysis of solar chimney power plant (SCPP): a review. Sustain. Energy Technol. Assess. 47, 101411.

Rabehi, R., Chaker, A., Ming, T., Gong, T., 2018. Numerical simulation of solar chimney power plant adopting the fan model. Renew. Energy 126, 1093–1101. https://doi.org/10.1016/j.renene.2018.04.012.

Salari, A., Shakibi, H., Alimohammadi, M., Naghdbishi, A., Goodarzi, S., 2023. A machine learning approach to optimize the performance of a combined solar chimney-photovoltaic thermal power plant. Renew. Energy 212, 717–737. https://doi.org/10.1016/j.renene.2023.05.113.

Salim, M.H., Schubert, S., Resler, J., Krč, P., Maronga, B., Kanani-Sühring, F., Sühring, M., Schneider, C., 2022. Importance of radiative transfer processes in urban climate models: a study based on the PALM 6.0 model system. Geosci. Model Dev. 15, 145–171. https://doi.org/10.5194/gmd-15-145-2022.

Spiegel, E.A., Veronis, G., 1960. On the Boussinesq approximation for a compressible fluid (Mar). Astrophys. J. 131, 442.

Toghraie, D., Karami, A., Afrand, M., Karimipour, A., 2018. Effects of geometric parameters on the performance of solar chimney power plants. Energy 162, 1052–1061.

Ulucak, O., Kocak, E., Bayer, O., Beldek, U., Yapıcı, E.Ö., Aylı, E., 2021. Developing and implementation of an optimization technique for solar chimney power plant with machine learning. J. Energy Resour. Technol. 143 (5), 052109. https://doi.org/10.1115/1.4049002.

Yapıcı, E.Ö., Ayli, E., Nsaif, O., 2020. Numerical investigation on the performance of a small scale solar chimney power plant for different geometrical parameters. J. Clean. Prod. 276. https://doi.org/10.1016/j.jclepro.2020.122908.

Yaswanthkumar, A., Chandramohan, V.P., 2019. Numerical analysis of flow parameters on solar updraft tower (SUT) with and without thermal energy storage (TES) system. J. Therm. Anal. Calor. 136 (1), 331–343. https://doi.org/10.1007/s10973-018-7756-z.

Zou, Z., He, S., 2015. Modeling and characteristics analysis of hybrid cooling-tower-solar-chimney system. Energy Convers. Manag 95, 59–68. https://doi.org/10.1016/j.enconman.2015.01.085.